RSC Advances

PAPER

View Article Online
View Journal | View Issue

Cite this: *RSC Adv.*, 2020, **10**, 40597

Insights into the impurities of Bi_2WO_6 synthesized using the hydrothermal method

Jiayou Liu,[ab] Qianqian Nie,[abc] Zhongchao Tan,[c] Yulin Luo,[d] Shuai Wang[d] and Hesheng Yu*[ab]

Bismuth tungstate (Bi_2WO_6) nanomaterials are widely used as visible-light driven photocatalysts. However, limited attention has been paid to the purity of prepared Bi_2WO_6 nanoparticles, which may affect the photocatalytic performance and hinder in-depth study of Bi_2WO_6. In this work, the impurities of Bi_2WO_6 formed during the hydrothermal process under a wide range of acid–base conditions (from 1.5 M HNO_3 to 0.5 M NaOH) were qualitatively analyzed and accurately quantified for the first time. After confirmation of Bi_2WO_6 stability, the impurities were dissolved using acid or base treatment, followed by measurements of the ion concentrations using Inductively Coupled Plasma Mass Spectrometry (ICP-MS). Furthermore, various characterization techniques including XRD, FE-SEM, TEM, UV-Vis DRS, XPS and FTIR were implemented to explore the change in morphology and optical properties of Bi_2WO_6 prepared in different acid–base environments, and to facilitate qualitative analysis of impurities. The hydrolytic properties of raw materials used for the synthesis of Bi_2WO_6 were also analyzed with UV-Vis transmittance observation. Following these analyses, the types and contents of impurities in Bi_2WO_6 prepared by the hydrothermal method under different acid–base conditions were determined. Results show that the primary impurity is $WO_3 \cdot 0.33H_2O$ (41.09%) for the precursor prepared in 1.5 M nitric acid solution. When the pH of the precursor was in the range of 0.97–7.01, the synthesized Bi_2WO_6 has relatively high purity, and the impure products were identified as $BiONO_3$. Bi_2O_3 began to appear when pH reached 9.01 and it reached 18.88% when pH was 12.98. The final product was Bi_2O_3 exclusively for the precursor conditioned in 0.5 M NaOH solution. In addition, the accuracy of the proposed quantitative method using ICP-MS was validated for several scenarios by weight difference experiments.

Received 3rd September 2020
Accepted 31st October 2020

DOI: 10.1039/d0ra07559k

rsc.li/rsc-advances

1. Introduction

Many researchers consider photocatalysis to be a promising technology for sustainable energy production and environmental remediation. Photocatalysts such as TiO_2,[1] ZnO[2] and SnO_2 [3] have been extensively studied; however, such catalysts only respond to the ultraviolet light because of their wide band gaps. Meanwhile, ultraviolet light accounts for approximately 4%[4] of the solar energy on the surface of the planet earth and 44% of sunlight is visible. As a result, visible-light responsive photocatalysts with a narrow band gap have attracted growing interest in research.

Bismuth tungstate (Bi_2WO_6) has recently gained considerable attention because of its physicochemical stability and efficient response to visible light.[5] Bi_2WO_6 and its modified catalysts have been used for degradation of organic wastewater, conversion of carbon dioxide (CO_2), water splitting for hydrogen production, and removal of nitric oxide (NO) from atmosphere.[6–11] Since Kudo[12] first synthesize Bi_2WO_6 by conventional solid state reactions, many methods have emerged for its preparation including hydrothermal method,[13,14] microwave-[15] and ultrasonic-assisted[16] hydrothermal method, solvothermal procedure,[17] sol–gel process,[18] grinding and calcination,[19] and co-precipitation.[20] Among these methods, the hydrothermal method is one of the most widely used because of its simplicity, safety, and high yield.[21,22]

During the hydrothermal synthesis process, the final products may be affected by factors, such as hydrothermal reaction temperature and pH value of precursors. Zhang and Zhu[23] explored the impact of hydrothermal reaction temperature on the properties of Bi_2WO_6 nanocatalysts. They observed that the crystallinity and morphology of final products were affected by the temperature and time during hydrothermal process. Specifically, low temperature will lead to poor crystallinity, while high temperature will result in low photocatalytic activity. Additionally, it is well acknowledged that pH value also affects

[a]Key Laboratory of Coal Processing and Efficient Utilization, Ministry of Education, Xuzhou 221116, China. E-mail: heshengyu@cumt.edu.cn
[b]School of Chemical Engineering and Technology, China University of Mining and Technology, Xuzhou 221116, China
[c]Department of Mechanical & Mechatronics Engineering, University of Waterloo, 200 University Avenue West, Waterloo N2L 3G1, Canada
[d]Advanced Analysis and Computation Center, China University of Mining and Technology, Xuzhou 221116, China

several physical properties of Bi_2WO_6 in a hydrothermal preparation. Huang *et al.*[24] produced Bi_2WO_6 nanomaterials with different morphologies by adjusting the pH level of the precursor solution. At pH 8, the fluffy microspheres-like Bi_2WO_6 exhibited the highest photocatalytic activity. Hu *et al.*[25] reported that the pH value of precursor solution affected the specific surface area and the porosity of their Bi_2WO_6 nanocatalysts. Lin *et al.*[14] reported that pH value impacted on the particle sizes of the synthesized Bi_2WO_6 photocatalysts. Moreover, the pH value of precursor could affect the composition of final products. Some researchers prepared WO_3/Bi_2WO_6 composite in a strong acid environment.[26,27] Others discovered $Bi_{3.84}W_{0.16}O_{6.24}$ in Bi_2WO_6 nanomaterials prepared under alkali conditions.[28] Therefore, it is likely that the acidity and/or alkalinity of preparation conditions may have a strong impact on the final products. However, most researchers focused on properties like morphology and specific surface area; few attempted to determine the purity of Bi_2WO_6 nanomaterials prepared at different synthesis conditions.

It is therefore necessary to qualitatively and quantitatively analyze impurities to better understand the effects of synthesis conditions on the purity of Bi_2WO_6. The impure components in Bi_2WO_6 can be qualitatively analyzed by some characterization technologies such as XRD, SEM and FTIR.[29,30] Earlier studies have indicated that the impurities in Bi_2WO_6 prepared *via* hydrothermal method mainly resulted from the hydrolysis of raw materials.[26,31,32] Therefore, accurate and comprehensive understanding of the hydrolysis properties of $Bi(NO_3)_3\cdot 5H_2O$ and $Na_2WO_4\cdot 2H_2O$ at different pH levels is also essential to qualitative analysis of impurities.

To the best of our knowledge, however, there is not relevant research on the quantification of impurities in Bi_2WO_6 nanomaterials. One feasible strategy is to take advantage of the difference in physio-chemical properties between impurities and Bi_2WO_6. As far as we know, the hydrolysate of the raw material for Bi_2WO_6 preparation can be dissolved in an acid or hot alkali solution,[33,34] while Bi_2WO_6 is relatively stable.[35,36] Hence it is reasonable to carry out quantitative analysis by dissolving impurities from the Bi_2WO_6 samples.

The objective of the current work is to study the impurities of prepared Bi_2WO_6 nanocatalysts. For this purpose, we first synthesized Bi_2WO_6 using hydrothermal method from 1.5 M nitric acid (HNO_3) to 0.5 M sodium hydroxide (NaOH) solutions. Then we identified the compounds of the impurities and other properties of the samples according to XRD, UV-Vis DRS, XPS FTIR, FE-SEM, TEM results and hydrolysis properties of raw materials for preparation of Bi_2WO_6. After that, the stability of Bi_2WO_6 was determined experimentally to ensure the feasibility of quantitative experiments. Later, impurities in the catalysts were dissolved into strong acid or hot alkaline solutions. Following that, the concentrations of key elements in the solutions were measured using ICP-MS, followed by conversion into mass weight of corresponding impurities. Finally, the accuracy of the quantitative method based on the ICP-MS technique was then verified by weight difference experiments. Overall, the present work is expected to shed light onto Bi_2WO_6-related studies and investigations using $Bi(NO_3)_3\cdot 5H_2O$ and/or $Na_2WO_4\cdot 2H_2O$ as raw materials.

2. Experimental

2.1 Materials

Reagents used in this research include $Bi(NO_3)_3\cdot 5H_2O$ (≥99.0%), $Na_2WO_4\cdot 2H_2O$ (≥99.5%), ethanol (≥99.7%), NaOH (≥96.0%) and concentrated HNO_3 (65–68.0%). They are all of analytical grade and were purchased from Sinopharm Chemical Reagent Co. These chemicals were used as received without further purification. Ultrapure water with a resistivity of 18.2 MΩ cm^{-1} produced by Direct-Q 5 UV System (Merck Millipore Germany) was used in this study.

2.2 Synthesis of Bi_2WO_6 in different acid and alkali conditions

The Bi_2WO_6 nanomaterials were prepared using hydrothermal method. The molar ratio between bismuth and tungstate was maintained at 2 : 1. The preparation procedures of precursor suspension under strong acid or mild alkali condition differs slightly from those under dilute acid and base conditions. To prepare Bi_2WO_6 under strong acid condition, 1.0914 g of bismuth nitrate pentahydrate ($Bi(NO_3)_3\cdot 5H_2O$) and 0.3711 g of sodium tungstate dihydrate ($Na_2WO_4\cdot 2H_2O$) were first weighed using an analytical balance (METTLER TOLEDO-ME104E/02). They were then transferred to two beakers containing 30 mL of nitric acid solution, the concentration of which ranged from 0.5 M to 1.5 M. These two solutions were magnetically stirred for 30 minutes separately, before they were mixed up for another 20 minutes. Nanomaterials synthesized under such strong acid conditions are denoted as 0.5MHNO, 1.00MHNO, 1.25MHNO, and 1.5MHNO; the numerical numbers stand for HNO_3 concentrate. As for mild base condition, the same amount of $Bi(NO_3)_3\cdot 5H_2O$ and $Na_2WO_4\cdot 2H_2O$ were dissolved in 30 mL of 0.5 M NaOH solution, respectively. The subsequent procedures are the same as those under strong acid conditions and the corresponding nanomaterials are denoted as 0.5MNAOH.

For dilute acid and base conditions ranging from pH 0.97 to pH 12.98, 1.4552 g of $Bi(NO_3)_3\cdot 5H_2O$ and 0.4948 g of $Na_2WO_4\cdot 2H_2O$ were dissolved in 25 mL of 0.3 M HNO_3 solution and in 55 mL of ultrapure water, respectively. These two solutions were then magnetically stirred for 30 minutes separately, before they were mixed up for another 20 minutes. The pH of the precursor, which was monitored by a pH meter (S470-K, METTLER TOLEDO), was then adjusted to 0.97, 2.99, 4.99, 7.01, 9.01, 10.00, 11.05, 12.01 and 12.98 with NaOH and/or HNO_3. The corresponding nanomaterials synthesized under these conditions are defined as 0.97BWO, 2.99BWO, 4.99BWO, 7.01BWO, 9.01BWO, 10.00BWO, 11.05BWO, 12.01BWO, and 12.98BWO, respectively.

The precursor suspension was then transferred to a 100 mL PTFE autoclave, and heated at 180 °C for 24 h. After naturally cooling down to room temperature, the solid was collected by centrifuge, followed by washing 3 times with ultrapure water and ethanol, respectively. The nanomaterials collected were

then dried at 60 °C for 12 h; the resultant nanomaterials were stored for subsequent use.

2.3 Sample characterization

Crystal phase of the prepared photocatalysts was analyzed by the X-ray diffraction technique (XRD, Bruker AXS D8 Advance, Cu Kα, $\lambda = 1.5406$ Å, 40 kV, 40 mA) at 2θ angles from 5 to 80°,and a scan speed of 10° per min. Their optical properties were determined using UV-Vis diffused reflectance spectra (UV-Vis DRS, Hitachi U-3900H) over the wavelengths in the range of 275–800 nm. X-ray photoelectron spectroscopy (XPS) was performed on ESCALAB 250Xi using Al Kα radiation to determine the chemical valence and relative percentage of surface elements. The data of binding energy for all samples were calibrated with the C 1s signal at 284.8 eV. Field emission scanning electron microscope (FE-SEM, Hitachi-SU8220), which was operated at 10 kV acceleration voltage and 9800 nA emission current, was used to observe the morphology of the samples. Additionally, transmission electron microscopy (TEM) and high-resolution transmission electron microscopy (HR-TEM) observations were carried out on a Tecnai G2 F20 instrument in the bright field. Furthermore, chemical bonds of samples were determined using Fourier Transform Infrared Spectroscopy (FTIR, Bruker Vertex 80v) over the range of 400–4000 cm^{-1}.

2.4 Observation of critical point of hydrolysis

The raw materials [$Bi(NO_3)_3 \cdot 5H_2O$ and $Na_2WO_4 \cdot 2H_2O$] used for the preparation of Bi_2WO_6 were subject to severe hydrolysis in solution, producing insoluble precipitates.[9,27,31] The hydrolysis reactions contribute largely to the impurities in the Bi_2WO_6 produced during hydrothermal process. Therefore, understanding the hydrolysis properties of Bi^{3+} and WO_4^{2-} ions at different pH levels is important to impurity analysis.

The critical pH value of hydrolysis is defined as the pH value at which ions begin to hydrolyze. The critical pH values for Bi^{3+} and WO_4^{2-} ions were determined using the transmittance pattern of the UV-Vis spectrophotometer (Hitachi U-3900H). The precipitate may affect the transmittance intensity of a solution. Therefore, transmittance observations can be used to identify the critical pH values. At the critical pH value, transmittance drops abruptly due to the presence of precipitates.

The procedure of UV-Vis transmittance observation was described as follows. Firstly, $Bi(NO_3)_3$ and Na_2WO_4 were completely dissolved in a strong acidic solution and ultrapure water, respectively. The obtained transparent $Bi(NO_3)_3$ and Na_2WO_4 solutions were then gradually regulated using NaOH and HNO_3 solutions to reach a series of pH values with a small interval. The transmittance of these $Bi(NO_3)_3$ and Na_2WO_4 solutions was recorded at each pH value.

2.5 Catalysts stability

A new approach based on acid and base treatment is proposed herein to quantify the impurities in the Bi_2WO_6 nanomaterials produced by hydrothermal method. In this method, it is critical to ensure Bi_2WO_6 stability in the corresponding acid and base environments. For this purpose, 0.97BWO nanomaterials were treated with acid and alkaline solutions, respectively, following the same procedure as described in ICP-MS analysis, which can be found in the next section. Crystal structure stability and morphology stability were analyzed by examining the XRD patterns and FE-SEM images of 0.97BWO before and after treatment with acid or base solvents. In addition, chemical stability was observed based on the change in the mass of dissolved Bi and W elements during a period of 7 days.

Nanomaterials prepared at strong acid (1.5MHNO) and base (12.98BWO) precursors were also analyzed to further confirm the stability of Bi_2WO_6. The XRD patterns and FE-SEM images of 1.5MHNO before and after alkali treatment was compared. The stability of 12.98BWO was confirmed by XRD results before and after soaking with acid.

2.6 Quantitative analysis of impurities

Upon confirmation of Bi_2WO_6 stability, Inductively Coupled Plasma Mass Spectrometry (ICP-MS, Agilent 7900) was used to determine the soluble bismuth and tungstate ions dissolved in solutions. Data is used for the quantification of impurities in the Bi_2WO_6 nanomaterials synthesized under different acid and alkali conditions. The samples for ICP-MS analysis were prepared following these steps: for those prepared at pH value equal to or above 0.97, and the 0.5MNAOH nanomaterials, samples were soaked in pH 0.5 HNO_3 solution for one week to dissolve potential acid-soluble impurities. However, 1.5MHNO, 1.25MHNO, 1.00MHNO, 0.5MHNO and 0.97BWO samples were treated by boiling 0.5 M NaOH solution for 1 min to dissolve alkali-soluble impurities. The resultant suspension was separated by a centrifuge operating at 4500 rpm for 3 min; then the supernatant was then sampled and diluted for ICP-MS analysis.

The ICP-MS results were further verified by weight difference tests. A specific amount of 1.5MHNO, 0.97BWO and 12.98BWO samples were treated using base or acid solution. The treated catalysts were then cleaned in a sintered disc filter. The 1.5MHNO nanomaterials after alkaline treatment were washed using ultrapure water during filtration. However, the 0.97BWO, 12.98BWO samples soaked in acid were washed 5 times using pH 0.5 HNO_3 solution, followed by a thorough rinse with ultrapure water. This way, the hydrolysis of Bi^{3+} ions left on solids could be prevented, ensuring the accuracy of final analysis. After drying at 60 °C for 12 hours, the weight difference before and after acid or base treatment was recorded.

3. Results and discussion

3.1 XRD patterns of Bi_2WO_6 nanomaterials

Fig. 1 and 2 show the XRD patterns of the catalysts prepared under different acid and base conditions. All samples, except for 12.98BWO and 0.5MNAOH, exhibited diffraction peaks that match up with Bi_2WO_6 standard card (JCPDS No.: 39-0256). The peaks appear to be sharp, indicating that the primary compound of the samples is highly crystalline Bi_2WO_6. Fig. 1 also shows that the phase of $WO_3 \cdot 0.33H_2O$ (JCPDS No.: 35-0270)

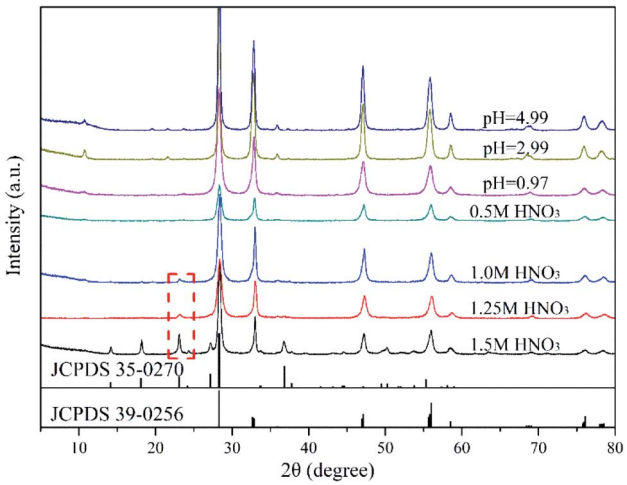

Fig. 1 XRD patterns of the catalyst synthesized in acidic environment.

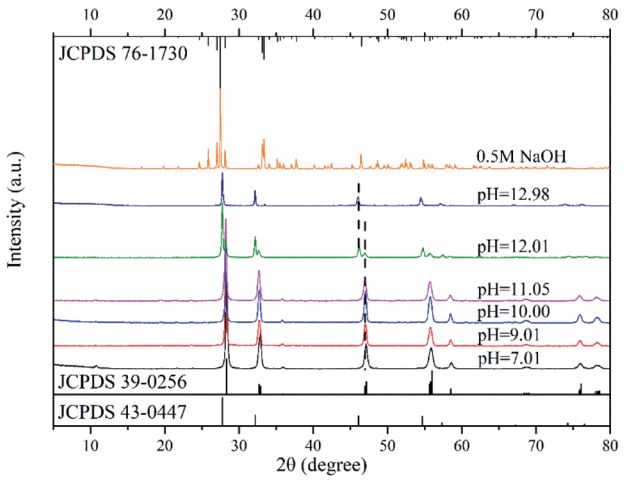

Fig. 2 XRD patterns of the catalyst synthesized in alkaline environments.

is present in the nanomaterials synthesized in strong acid environments including 1.5 M, 1.25 M, and 1.0 M HNO_3 solutions. The presence of $WO_3 \cdot 0.33H_2O$ is consistent with the results of SEM analysis in the following section. In such cases, the H^+ ion concentrations in the precursor were so high that WO_4^- ions combined with H^+ to produce insoluble precipitation of H_2WO_4. H_2WO_4 then dehydrated during the hydrothermal process to generate $WO_3 \cdot 0.33H_2O$. However, it was difficult to observe the peaks of $WO_3 \cdot 0.33H_2O$ in the XRD spectrum of the 0.5MHNO samples. The samples of 0.5MHNO, 0.97BWO, 2.99BWO, and 4.99BWO showed only characteristic peaks of Bi_2WO_6, and the intensity of the strongest (131) peak at 28.299° changed significantly from about 1572 to about 10 631 as the acidity decreased. This finding might be attributed to the increase in crystallite size and enhanced crystallinity perfection.[28]

Fig. 2 shows the XRD patterns of catalysts synthesized in neutral and alkaline environments. For pH values ranging from 7.01 to 11.05, the XRD spectrums showed the phase of Bi_2WO_6 only. When the pH value increased to 12.01, however, a new crystal phase of $Bi_{3.84}W_{0.16}O_{6.24}$ (JCPDS No.: 43-0447), besides Bi_2WO_6, appeared in the prepared nanomaterials. Moreover, the intensity of the diffraction peak of $Bi_{3.84}W_{0.16}O_{6.24}$ was stronger than that of Bi_2WO_6. This may be attributed to the solubility of $[WO_4]^{2-}$ in the precursor suspension, which is much greater than that of $[Bi_2O_2]^{2+}$ in a strong alkaline environment. Therefore, $[Bi_2O_2]^{2+}$ can precipitate rapidly, forming the new phase of $Bi_{3.84}W_{0.16}O_{6.24}$.[28,37] As the pH value reached 12.98, however, the phase of Bi_2WO_6 disappeared and only $Bi_{3.84}W_{0.16}O_{6.24}$ existed. In this paper, $Bi_{3.84}W_{0.16}O_{6.24}$ is regarded as another crystalline phase of Bi_2WO_6 rather than impurities because of its strong stability and catalytic ability. Synthesized $Bi_{3.84}W_{0.16}O_{6.24}$ could be converted to α-Bi_2O_3 (JCPDS No.: 76-1730) when the precursor was further conditioned by 0.5 M NaOH solution. The formation of α-Bi_2O_3 resulted from the high concentration of OH^- in the precursor, leading to the production of $Bi(OH)_3$. $Bi(OH)_3$ further transformed into α-Bi_2O_3 under hydrothermal reaction conditions.[38] Consequently, Bi^{3+} ions were unable to participate in the synthesis of $Bi_{3.84}W_{0.16}O_{6.24}$ and Bi_2WO_6 with WO_4^{2-}.

According to the XRD patterns, $WO_3 \cdot 0.33H_2O$, $Bi_{3.84}W_{0.16}O_{6.24}$, and α-Bi_2O_3 were observed sequentially with increasing precursor alkalinity in addition to Bi_2WO_6. The results not only demonstrated the successful synthesis of Bi_2WO_6, but also strongly proved that different substances could be produced under different acid–base conditions.

3.2 Optical properties of catalysts

The UV-Vis DRS was used to determine the photo-response range of nanomaterials synthesized under different acid and alkali conditions. It can be seen from Fig. 3 that all samples showed high photo-absorption at around 380 nm, and their absorption bands were approximately 450 nm. This indicates that all the synthesized samples are responsive to visible light

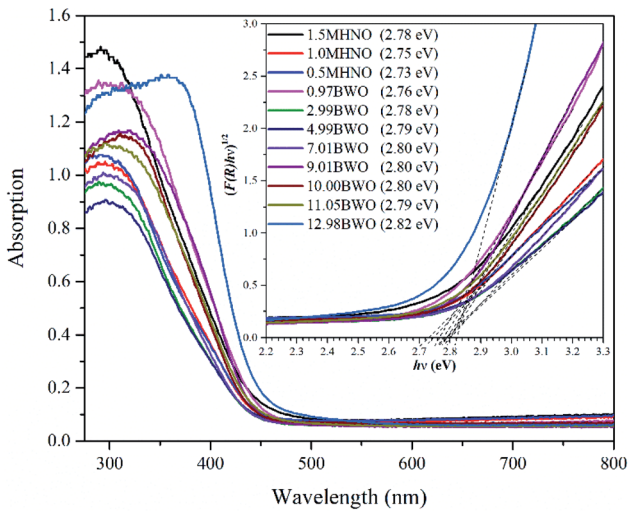

Fig. 3 UV-Vis DRS spectra of photocatalysts synthesized in different acid and base conditions.

regardless of the pH value of the precursor. In addition, the optical band gap of the as-prepared photocatalysts were calculated using Kubelka–Munk (KM) method,[39] and the results are included in the legend of Fig. 3.

Fig. 3 shows that the band gaps of different catalysts, including 0.97BWO, 2.99BWO, 4.99BWO, 7.01BWO, 9.01BWO, 10.00BWO and 11.05BWO, varied slightly between 2.76–2.80 eV. This range is consistent with those in other studies on Bi_2WO_6.[40,41] The absorption edges of 1.5MHNO, 1MHNO and 0.5MHNO are 446 nm, 451 nm and 454 nm corresponding to band gaps of 2.78 eV, 2.75 eV and 2.73 eV, respectively. The band gap of 12.98BWO (which is $Bi_{3.84}W_{0.16}O_{6.24}$) is 2.82 eV, corresponding to previous report as well.[42] The results in this section indicate that all samples have visible light response capabilities and that the band gap lies between 2.73 eV and 2.82 eV.

3.3 Morphology and structure of prepared nanomaterials

Morphologies of the samples were characterized by FE-SEM and TEM techniques. It can be seen from Fig. 4a that the 1.5MHNO sample appears like a flower with dewdrops. Specifically, the flower-like base is made up with large nanosheets, which are decorated by small "nanocrumbs". The large nanosheets are composed of Bi_2WO_6 and the nanocrumbs are $WO_3 \cdot 0.33H_2O$. The presence of these two substances is further confirmed with the XRD pattern of 1.5MHNO. As the acidity decreases, regular large nanosheets disappear, and are replaced by irregular flocs consisting of small nanosheets for precursor prepared in 0.5 M HNO_3 solution (Fig. 4b). Fig. 4c shows the morphology of Bi_2WO_6 prepared at pH 0.97. Numerous small nanosheets accumulate to form large wheat spike-like shapes (see the inset on the top right). Further accumulation of these spike-like structures resulted in 3D spheres, the diameters of which are about 4–7 μm.

The morphologies of the synthesized catalysts are similar to each other when the pH values of the precursors fall into the range of 4.99–7.01 (Fig. 4d and e). Both appear to be building blocks, formed by interspersion between small rectangular pieces. The side lengths of these blocks are approximately 0.6–1.0 μm. The lower the acidity is, the thicker the blocks are.

Fig. 4f and g illustrate that the shapes of samples 9.01BWO and 11.05BWO are like square bricks. These square bricks of Bi_2WO_6 are randomly plied up without obvious aggregation. As the pH value reaches 12.01, a new crystal phase of $Bi_{3.84}W_{0.16}O_{6.24}$ emerges. Two different morphologies can be clearly observed in Fig. 4h. The sheet shape is for the Bi_2WO_6 and the regular octahedron shape is for $Bi_{3.84}W_{0.16}O_{6.24}$. It also shows that the $Bi_{3.84}W_{0.16}O_{6.24}$ crystal is the dominate phase. This finding agrees with the XRD patterns of 12.01BWO samples presented in Fig. 2, which show two crystal phases.

Fig. 4i shows the morphology of 12.98BWO nanomaterials. It does not show the structure of the Bi_2WO_6 sheet, but regular octahedral crystals of $Bi_{3.84}W_{0.16}O_{6.24}$ and some irregular small crystals. According to the FTIR results in the following section and those in earlier studies,[31,38] these irregular crystals are likely Bi_2O_3. Finally, the synthesized crystals become irregular Bi_2O_3 spheres and rods with various sizes when the precursor is conditioned using 0.5 M NaOH solution (Fig. 4j). The transformation arises from the fact that a large amount of OH^- ions in the precursor directly combines with Bi^{3+} ions to form $Bi(OH)_3$, which is then converted into Bi_2O_3 after dehydration during hydrothermal process.[43]

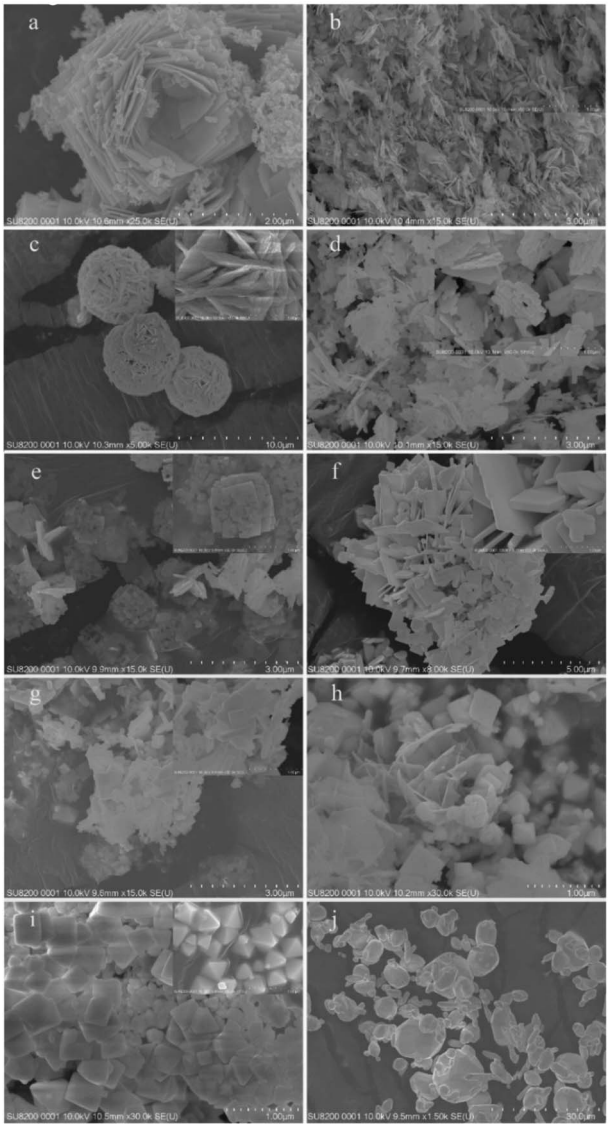

Fig. 4 SEM images of samples synthesized at different acid and alkali environments: (a) 1.5MHNO; (b) 0.5MHNO; (c) 0.97BWO; (d) 4.99BWO; (e) 7.01BWO; (f) 9.01BWO; (g) 11.05BWO; (h) 12.01BWO; (i) 12.98BWO; (j) 0.5MNAOH.

Fig. 5 presents the TEM images of 1.5MHNO and 12.01BWO samples. The overall TEM image of 1.5MHNO in Fig. 5a shows large nanosheets decorated by small "nanocrumbs". The section inside the circle was further analyzed using HR-TEM (Fig. 5b), which reveals the lattice interplanar spacing (0.31 nm) of the large nanosheets corresponding to the (131) plane of Bi_2WO_6. The nanocrumbs sprinkled onto the large nanosheet have interplanar distances of 0.32 nm and 0.37 nm, corresponding to the crystal lattice spacing of the (220) and (200) planes of $WO_3 \cdot 0.33H_2O$, respectively. These findings are

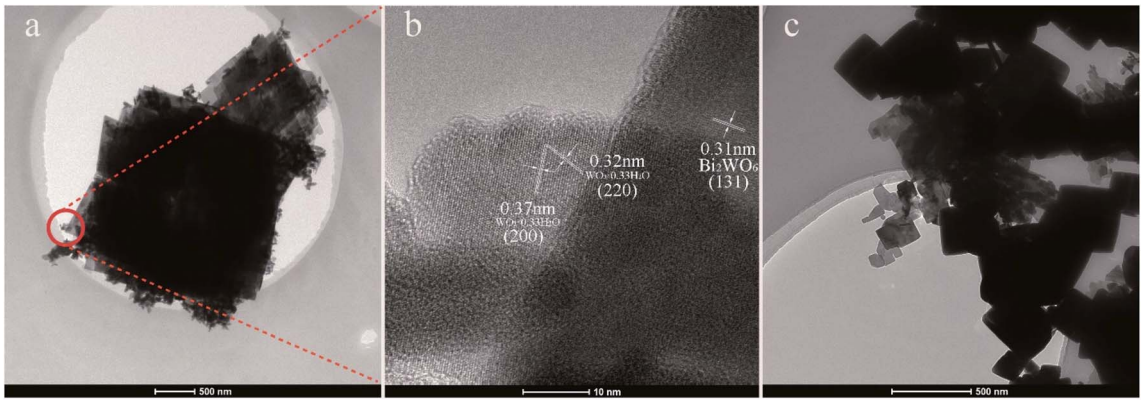

Fig. 5 TEM and HRTEM of samples: (a) TEM and (b) HRTEM of 1.5MHNO; (c) TEM of 12.01BWO.

consistent with the SEM image shown in Fig. 4a. Fig. 5c shows the TEM image of 12.01BWO. Both granular and flaky crystals can be clearly seen. These SEM and TEM images clearly show the change of morphology and transformation of dominate compounds with the variation from strong acid to mild base circumstances.

3.4 XPS analyses

Fig. 6 shows the percentage and chemical valence states of surface elements determined by XPS. The high-resolution XPS spectra of O 1s are shown in Fig. 6a. Through Gaussian distribution, the O 1s peaks of samples could be deconvoluted into three peaks at 529.19–529.87 eV, 529.91–530.46 eV and 531.10–532.34 eV. They are assigned to lattice oxygen, hydroxyl groups and H_2O molecules adsorbed on the samples surface.[11] Generally, a high ratio of the peak area of hydroxyl groups to that of lattice oxygen indicates a high concentration of oxygen vacancies.[44] According to this rule, it can be speculated that the concentration of oxygen vacancy depends upon the acidity of precursor environment. The 7.01BWO samples have the highest concentration of oxygen vacancy, while the 0.5MNAOH samples have the smallest one.

As shown in Fig. 6b, the spectrum of Bi 4f had two peaks located at around 158.74 eV and 164.05 eV, which correspond to Bi $4f_{7/2}$ and $4f_{5/2}$, respectively. Moreover, the difference between the two binding energies is about 5.31 eV, indicating the existence of Bi^{3+} in all samples.[10] In Fig. 6c, the peaks around 34.96

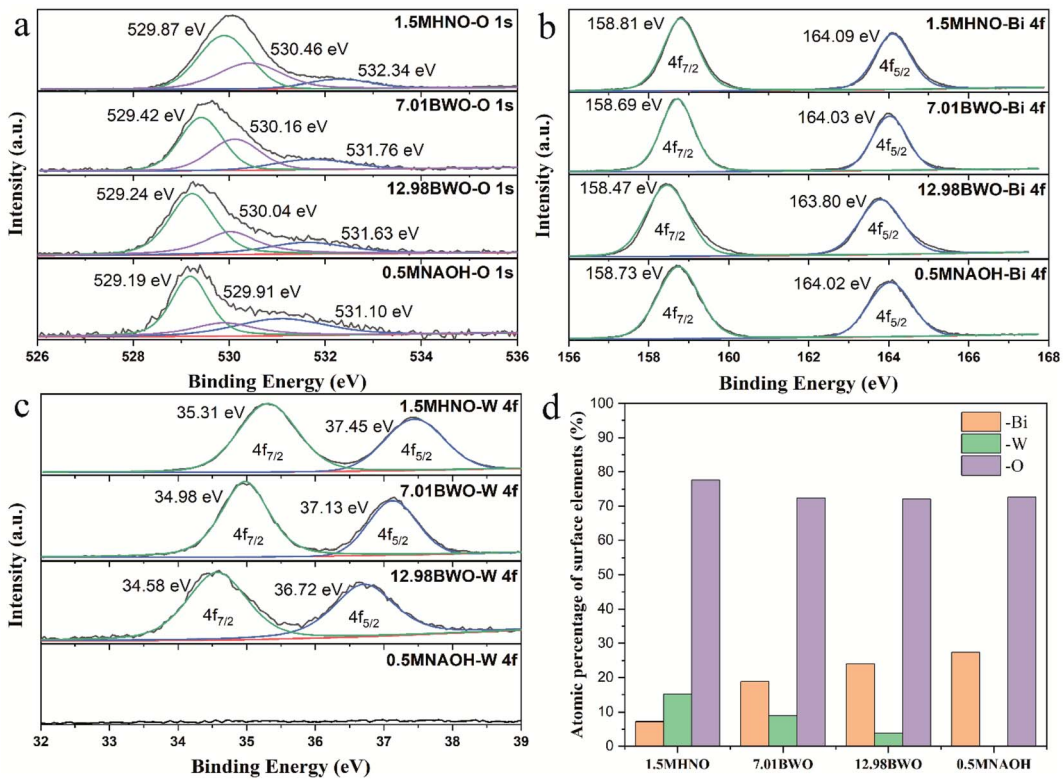

Fig. 6 High-resolution XPS spectrums of (a) O 1s, (b) Bi 4f and (c) W 4f of samples; (d) atomic percentage of surface elements on samples.

and 37.10 eV are fitted into W $4f_{7/2}$ and $4f_{5/2}$, respectively. The peak distance of 2.14 eV indicates that W in these samples are mainly presented as W^{6+}.[45] Moreover, the absence of W peaks in the 0.5MNAOH sample confirms that 0.5MNAOH samples are Bi_2O_3.

Fig. 6d shows the XPS atomic percentage of surface elements on different samples. The content of O element changes insignificantly with the variation in precursor acidity. When the acidity gradually increases, the W element gradually increases, whereas the Bi element gradually decreases. This finding is associated with gradual transformation of the main substances from Bi_2O_3 into $Bi_{3.84}W_{0.16}O_{6.24}$, into Bi_2WO_6, and into Bi_2WO_6/$WO_3 \cdot 0.33H_2O$ with increasing acidity.

3.5 FTIR analyses

Fig. 7 shows the FTIR spectra of the as-prepared samples. The absorption peaks mainly range from 400 to 1000 cm^{-1}. Specifically, the adsorption band at 441 cm^{-1} and 578 cm^{-1} are owing to the bending vibrations of Bi–O bond; the strong peaks at 727 cm^{-1} and 820 cm^{-1} are attributed to the W–O and W–O–W bond of Bi_2WO_6, respectively.[16,46] These peaks prove the successful synthesis of Bi_2WO_6 nanomaterials.

The minor peaks at 1001 cm^{-1} and 1608 cm^{-1} of 1.5MHNO's FTIR spectrum are assigned to the W=O valence vibrations and δ(O–H) stretching vibrations of coordinated water, respectively. They are likely attributed to the crystal phase of $WO_3 \cdot 0.33H_2O$.[47] Additionally, the weak peak at 1634 cm^{-1} corresponds to the O–H bond of the adsorbed water molecules.[48] The peaks at 500 cm^{-1} and 787 cm^{-1} are likely originated from the vibrations of Bi–O and W–O bonds of $Bi_{3.84}W_{0.16}O_{6.24}$. Unlike the characteristic peaks in Bi_2WO_6, the intensity of the Bi–O peak is greater than that of W–O. This may result from the increase of Bi–O bond in $Bi_{3.84}W_{0.16}O_{6.24}$.

It is worth noting that the small peak at 1384 cm^{-1} corresponds to the vibration of N–O bond.[46,48] It was ascribed to the hydrolysis products of $Bi(NO_3)_3 \cdot 5H_2O$, such as $BiONO_3$ and $Bi_2O_2(OH)NO_3$.[31,49] This conclusion can also be verified by comparing the FTIR spectra of 0.97BWO before and after the acid treatment. After acid soaking, most of the impurities ($BiONO_3$ and $Bi_2O_2(OH)NO_3$) in 0.97BWO was dissolved, which corresponds to a sudden decrease in the peak at 1384 cm^{-1} while others remained almost unchanged. This peak becomes weaker with the increasing alkalinity, and it disappears at pH 9.01. With the escalation of OH^- concentration in the precursor, $BiONO_3$ and $Bi_2O_2(OH)NO_3$ gradually transform into $Bi(OH)_3$, which could be further converted to Bi_2O_3 *via* hydrothermal reaction. Furthermore, the tiny peak at 1384 cm^{-1} of 1.5MHNO is probably due to the hydrolysis of minor residual of Bi^{3+} ions, which forms $BiONO_3$ precipitates on nanocatalyst surface during washing with ultrapure water.

The nanomaterials synthesized at pH value greater than 7.01 has no obvious peaks between 3400 cm^{-1} and 3800 cm^{-1}, which are the characteristic peaks of O–H.[50–52] It is believed that most $Bi(OH)_3$ was converted to Bi_2O_3, which is the main impurity at pH $\geq$ 9.01.

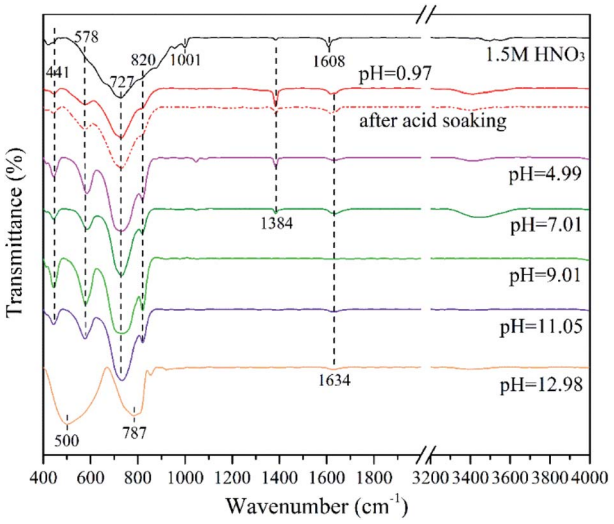

Fig. 7 The FTIR spectra of photocatalysts synthesized in different acid and base conditions.

3.6 Stability analysis

The stability of the prepared Bi_2WO_6 is evaluated in terms of crystal structure, morphology, and chemical composition. Fig. 8a shows the XRD patterns of original 0.97BWO and 0.97BWO before and after treatment with acid or base solutions, which shows that the three XRD patterns are barely affected by the treatment. They are almost the same, and can match the Bi_2WO_6 standard card (JCPDS No.: 39-0256) well. It indicates that the crystal structure of as-prepared Bi_2WO_6 is not damaged during the acid or base treatment.

On the contrary, Fig. 8b clearly demonstrates that XRD pattern of 1.5MHNO changes after alkali treatment. The disappearance of the characteristic peaks of $WO_3 \cdot 0.33H_2O$ impurity indicates that $WO_3 \cdot 0.33H_2O$ in 1.5MHNO can be dissolved in a boiling alkaline solution, but Bi_2WO_6 is stable. The disappearance of the "nanocrumbs" scattered on the flower-like Bi_2WO_6 in the inset SEM images supports this conclusion. For $Bi_{3.84}W_{0.16}O_{6.24}$ (Fig. 8c), XRD spectrum remains the same before and after acid leaching, indicating that $Bi_{3.84}W_{0.16}O_{6.24}$ is relatively stable.

The chemical stability of Bi_2WO_6 is verified by ICP-MS data. Fig. 8d shows the variation of Bi and W elements leached from 1 g of 0.97BWO sample over 7 days. As soaking time increases, the mass of dissolved Bi element in the HNO_3 solution at pH 0.5 first increased and then leveled off. Similar trend is observed for the change of W element dissolved in 0.5 M NaOH solution. The constant quantity of the leaching elements after 3 days strongly proves the chemical stability of Bi_2WO_6. Meanwhile, undamaged microspheres of 0.97BWO in the inset SEM images of Fig. 8d indicates morphological stability.

In summary, Bi_2WO_6 and $Bi_{3.84}W_{0.16}O_{6.24}$ are stable enough to resist dissolution during acid and base treatments. Therefore, the Bi and W elements measured by ICP-MS in the following leaching experiment are believed to be derived from soluble impurities rather than from Bi_2WO_6 and $Bi_{3.84}W_{0.16}O_{6.24}$.

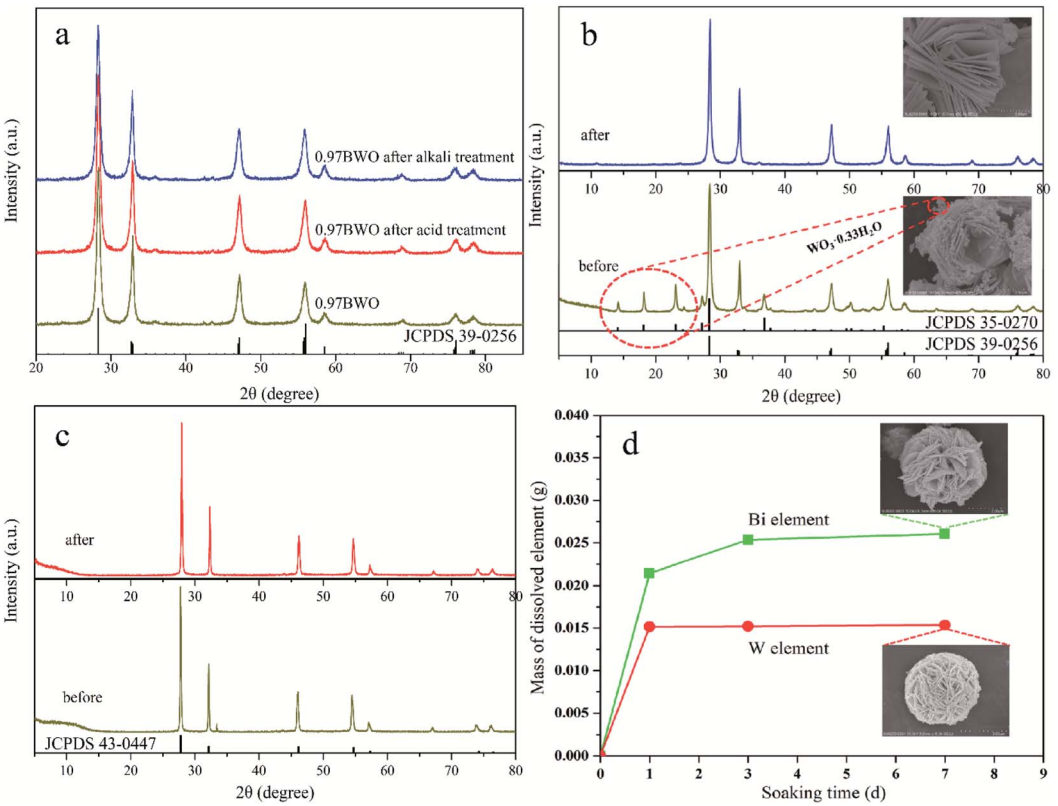

Fig. 8 (a) XRD of 0.97BWO and 0.97BWO after acid or alkali treatment; (b) XRD patterns and morphologies of 1.5MHNO before and after boiling alkali solution treatment; (c) XRD patterns of 12.98BWO before and after acid treatment; (d) mass of the Bi and W elements dissolved in acid or base solution, respectively, and the morphologies of 0.97BWO after acid or base treatment.

3.7 Determination of impurities

The impurities in Bi_2WO_6 prepared under a wide range of acid–base conditions were qualitatively analyzed according to the characterization results and hydrolysis properties of the raw materials. The mass percentage of impurities was calculated using ICP-MS results, and the accuracy was verified by several weight difference experiments.

3.7.1 Hydrolysis properties. The knowledge on the hydrolysis reactions of Bi^{3+} and WO_4^{2-} ions is critical to the analysis of possible impurities in the prepared nanomaterials. Fig. 9 shows the transmittances of $Bi(NO_3)_3$ solution and Na_2WO_4 solution at different pH values. According to Fig. 9a, it is observed that the critical pH is 0.67 for the hydrolysis of Bi^{3+} ion. When the pH value is less than 0.67, Bi^{3+} ion is present in a free state; otherwise, Bi^{3+} ion is subject to hydrolysis to form such precipitates as $BiONO_3$ and $Bi_2O_2(OH)NO_3$.[31] Fig. 9b shows that the critical pH value of hydrolysis of WO_4^{2-} is 1.13. When pH is greater than 1.13, WO_4^{2-} ion is at a free state in solution; otherwise, WO_4^{2-} begins to hydrolyze and forms H_2WO_4 precipitate.[53] In summary, there is not a pH value at which the precursor of the hydrothermal reaction is a clear solution at room temperature. And both ions are hydrolyzed at pH value between 0.67–1.13.

It is believed that the impurities in the Bi_2WO_6 nanomaterials prepared using hydrothermal reaction are primarily hydrolysis products and derivatives of Bi^{3+} and WO_4^{2-} ions. The primary impurities include $WO_3 \cdot 0.33H_2O$, $BiONO_3$, $Bi_2O_2(OH)NO_3$, and Bi_2O_3. Eqn (1)–(6) describe the formation of such impurities. When the pH of the precursor is lower than 1.13, WO_4^{2-} ions will combine with H^+ ions to form H_2WO_4, which is transformed to $WO_3 \cdot 0.33H_2O$ in the subsequent hydrothermal reaction (eqn (1) and (2)). Bi^{3+} ions are subject to hydrolysis to form $BiONO_3$ and $Bi_2O_2(OH)NO_3$ precipitates when the pH is greater than 0.67 (eqn (3) and (4)). Since the degree of hydrolysis in the second step (eqn (4)) is much lower than that in the first step (eqn (3)), the hydrolysis products of Bi^{3+} ions are mainly $BiONO_3$ instead of $Bi_2O_2(OH)NO_3$. In a relatively strong base solution, impurities could progressively turn to Bi_2O_3, which is transformed from $Bi(OH)_3$ (eqn (5) and (6)).

$$WO_4^{2-} + 2H^+ \rightarrow H_2WO_4 \quad (1)$$

$$H_2WO_4 \rightarrow WO_3 \cdot 0.33H_2O + 0.67H_2O \quad (2)$$

$$Bi(NO_3)_3 + H_2O \leftrightarrow BiONO_3 + 2HNO_3 \quad (3)$$

$$2BiONO_3 + H_2O \leftrightarrow Bi_2O_2(OH)NO_3 + HNO_3 \quad (4)$$

$$Bi(NO_3)_3 + 3OH^- \rightarrow Bi(OH)_3 + 3NO_3^- \quad (5)$$

$$2Bi(OH)_3 \rightarrow Bi_2O_3 + 3H_2O \quad (6)$$

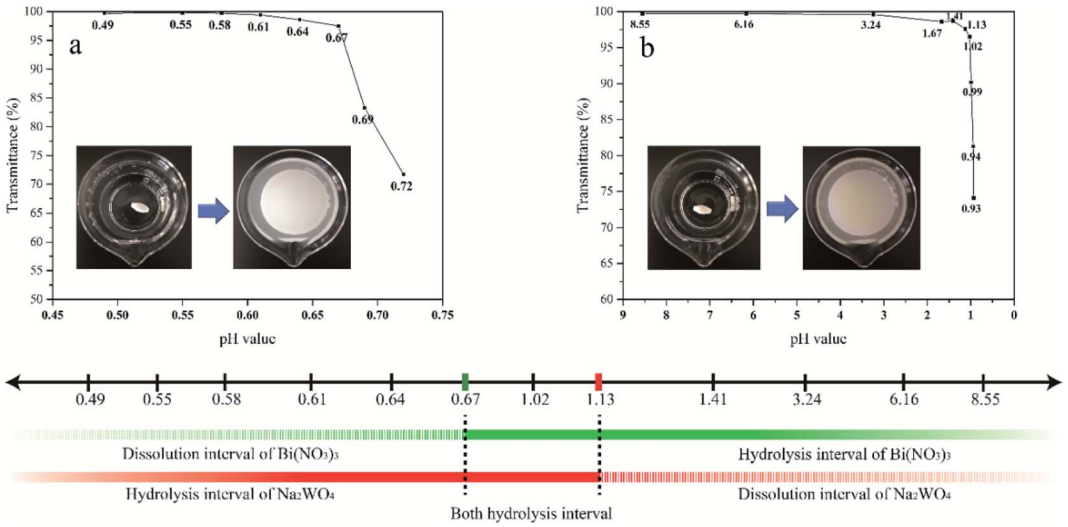

Fig. 9 Transmittance of (a) $Bi(NO_3)_3$ solution and (b) Na_2WO_4 solution at different pH values.

3.7.2 Qualitative analysis. The XRD patterns in Fig. 1 show that $WO_3 \cdot 0.33H_2O$ is the primary impurity in 1.5MHNO, 1.25MHNO, 1.00MHNO samples. Although the XRD pattern of 0.5MHNO does not show the phase of $WO_3 \cdot 0.33H_2O$, the WO_4^{2-} ions were observed using ICP-MS after the 0.5MHNO sample was treated in boiling NaOH solution. It indicates the existence of $WO_3 \cdot 0.33H_2O$ in the 0.5MHNO sample. The presence of $BiONO_3$ is unlikely, because Bi^{3+} ions do not hydrolyze in the pH value lower than 0.67 according to Fig. 9.

Fig. 9 indicates both Bi^{3+} and WO_4^{2-} ions can be hydrolyzed at pH 0.97. Their major hydrolysis products, $WO_3 \cdot 0.33H_2O$ and $BiONO_3$, could appear in the catalysts. The presence of $WO_3 \cdot 0.33H_2O$ is proven by ICP-MS measurements. The peak at 1384 cm^{-1} in the FTIR spectra confirms the presence of $BiONO_3$.

For the pH values between 2.99 and 7.01, the hydrolysis of WO_4^{2-} ions becomes negligible. $BiONO_3$, which is the predominant product of Bi^{3+} hydrolysis, constitutes to the impurity in the samples. The FTIR spectra of samples prepared within this pH range have a clear peak at 1384 cm^{-1}, indicating the existence of $BiONO_3$. As indicated by the FTIR results the hydrolysate $BiONO_3$ disappears when synthesizing catalyst under alkaline (pH $\geq$ 9.01) conditions. The presence of $Bi(OH)_3$ seems unlikely because there is not obvious vibration characteristic peak of O–H. Earlier studies indicate that impurities are very likely Bi_2O_3,[38,54–56] which could be converted from $Bi(OH)_3$ through hydrothermal reactions.

The Bi^{3+} ions were identified by ICP-MS after the 12.98BWO sample was soaked in acid solution, indicating the presence of acid soluble impurities. The aforementioned FTIR analysis proves that the acid-soluble impurity in 12.98BWO is likely Bi_2O_3. It is believed that the impurity is δ-Bi_2O_3 (ref. 57) because the positions of strong diffraction peaks of δ-Bi_2O_3 in XRD pattern (JCPDS No.: 27-0052 or JCPDS No.: 52-1007) are almost overlapping with those of the primary crystal phase of $Bi_{3.84}W_{0.16}O_{6.24}$.

Fig. 10 shows a concise diagram based on the preceding analyses presented to describe the transformation of samples and their impurities with the change of acid and alkali environments. Both the main compounds and the impurities in the samples undergo transformation. The main compounds begin to convert from Bi_2WO_6 to $Bi_{3.84}W_{0.16}O_{6.24}$ at precursor pH of around 12. Further increase in alkalinity leads to the production of Bi_2O_3. The impurities then gradually shift from $WO_3 \cdot 0.33H_2O$ to $BiONO_3$ around pH 1, and to Bi_2O_3 at near pH 7.

3.7.3 Quantitative analysis. Summarizes the mass ratio of corresponding impurities quantified using ICP-MS technique. The impurity of $WO_3 \cdot 0.33H_2O$ in the synthesized catalysts decreased from 41.09% to 1.99% as the acidity weakens from 1.5 M HNO_3 to pH 0.97. It is well known that high acidity favors the hydrolysis of WO_4^{2-} in the precursor. The higher the degree of WO_4^{2-} hydrolysis, the greater the content of $WO_3 \cdot 0.33H_2O$. When the pH value of the precursor solution is between 0.97 and 10.00, however, the content of impurity, which contains Bi^{3+} ions, in the synthesized catalyst does not change significantly. When the pH value increases to 11.05, the impurity content starts to increase exponentially, and all the hydrothermal reaction product was converted to Bi_2O_3 when the precursor prepared using 0.5 M NaOH solution. Sample 0.5MNAOH can be completely dissolved into the soaking solution of pH 0.5 HNO_3; therefore, it is deemed reasonable to conclude that no Bi_2WO_6 was produced in the sample. It is worth noting that the 0.97BWO sample contains both $WO_3 \cdot 0.33H_2O$ and $BiONO_3$, which confirms our previous assumption.

Weight difference experiments were conducted before and after purification to validate our identification analysis and the newly developed quantification method using ICP-MS. The results are tabulated in the last column of Table 1. ICP-MS provides similar results to the weight difference experiments. Most discrepancies are within 3.5%, except for the 12.98BWO samples, which is 11%. This indicates the analysis of impure

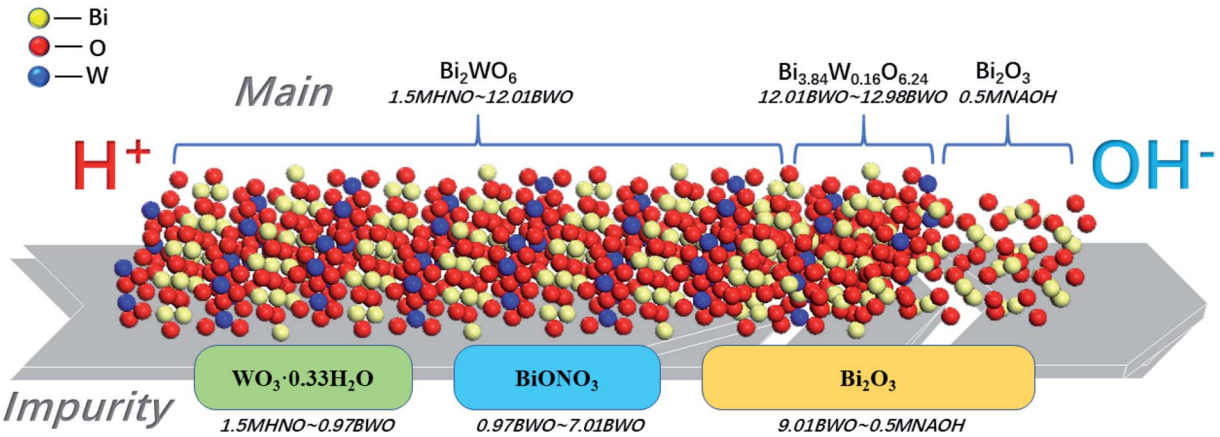

Fig. 10 Diagram of the transformation of the samples and their impurities with the change of acid and alkali environment.

Table 1 The mass fraction of impurities in various samples

Samples	Impurities	Mass weight (%) ICP-MS	Mass weight (%) weight difference experiment
1.5MHNO	$WO_3 \cdot 0.33H_2O$	41.09	39.75
1.25MHNO	$WO_3 \cdot 0.33H_2O$	14.27	—
1MHNO	$WO_3 \cdot 0.33H_2O$	9.90	—
0.5MHNO	$WO_3 \cdot 0.33H_2O$	5.99	—
0.97BWO	$WO_3 \cdot 0.33H_2O$/ $BiONO_3$	1.99/3.58	—/3.63
2.99BWO	$BiONO_3$	3.52	—
4.99BWO	$BiONO_3$	2.75	—
7.01BWO	$BiONO_3$	2.80	—
9.01BWO	Bi_2O_3	1.50	—
10.00BWO	Bi_2O_3	2.03	—
11.05BWO	Bi_2O_3	4.90	—
12.98BWO	Bi_2O_3	18.88	21.26
0.5MNAOH	Bi_2O_3	102.90	100.00

compounds and quantitative determination of impurities using ICP-MS method are reliable.

4. Conclusions

In summary, Bi_2WO_6 nanomaterials synthesized by hydrothermal methods in different acid–base environments all contain impurities. The pathway of impurities conversion with continuously changing acidity or alkalinity was determined. Strong acidity can lead to the formation of $WO_3 \cdot 0.33H_2O$ as impurities. Impurities such as $BiONO_3$, $Bi_2O_2(OH)NO_3$ and Bi_2O_3 appeared as the alkalinity increases. The synthesized catalysts had a relatively high purity when the pH of precursor is between 1 and 10. In addition, the as-prepared Bi_2WO_6 and $Bi_{3.84}W_{0.16}O_{6.24}$ nanomaterials were stable in both acid and base environments. Furthermore, this study provides a simple and feasible method to quantitatively analyze the impurity of Bi_2WO_6, which was verified by weight difference experiments. This work is expected to shed light onto Bi_2WO_6-related studies and investigations using $Bi(NO_3)_3 \cdot 5H_2O$ and/or $Na_2WO_4 \cdot 2H_2O$ as raw materials.

Conflicts of interest

There are no conflicts to declare.

Acknowledgements

This work is financially supported by "the Fundamental Research Funds for the Central Universities" (No.: 2019XKQYMS59). The authors would like to acknowledge the technical support from Advanced Analysis and Computation Center within China University of Mining and Technology.

References

1 M. Kong, Y. Li, X. Chen, T. Tian, P. Fang, F. Zheng and X. Zhao, *J. Am. Chem. Soc.*, 2011, **133**, 16414–16417.
2 T. J. Liu, Q. Wang and P. Jiang, *RSC Adv.*, 2013, **3**, 12662–12670.
3 H. L. Zhang and C. G. Hu, *Catal. Commun.*, 2011, **14**, 32–36.
4 Z. Li, W. Luo, M. Zhang, J. Feng and Z. Zou, *Energy Environ. Sci.*, 2013, **6**, 347–370.
5 B. Y. Alfaifi, A. A. Tahir and K. G. U. Wijayantha, *Sol. Energy Mater. Sol. Cells*, 2019, **195**, 134–141.
6 F. Ma, Q. Yang, Z. Wang, Y. Liu, J. Xin, J. Zhang, Y. Hao and L. Li, *RSC Adv.*, 2018, **8**, 15853–15862.
7 S. W. Cao, B. J. Shen, T. Tong, J. W. Fu and J. G. Yu, *Adv. Funct. Mater.*, 2018, **28**, 11.
8 J. Zhao, Y. Yang, X. Dong, Q. Ma, W. Yu, J. Wang and G. Liu, *RSC Adv.*, 2016, **6**, 64741–64748.
9 Y. Huang, Z. H. Ai, W. K. Ho, M. J. Chen and S. Lee, *J. Phys. Chem. C*, 2010, **114**, 6342–6349.
10 H. Huang, K. Liu, K. Chen, Y. Zhang, Y. Zhang and S. Wang, *J. Phys. Chem. C*, 2014, **118**, 14379–14387.
11 H. Huang, R. Cao, S. Yu, K. Xu, W. Hao, Y. Wang, F. Dong, T. Zhang and Y. Zhang, *Appl. Catal., B*, 2017, **219**, 526–537.
12 A. Kudo and S. Hijii, *Chem. Lett.*, 1999, **28**, 1103–1104.

13 Y. Y. Li, J. P. Liu, X. T. Huang and G. Y. Li, *Cryst. Growth Des.*, 2007, **7**, 1350–1355.
14 X. Lin, Z. X. Liu, X. Y. Guo, C. B. Liu, H. J. Zhai, Q. W. Wang and L. M. Chang, *Mater. Sci. Eng., B*, 2014, **188**, 35–42.
15 J. Huang, G. Tan, A. Xia, H. Ren and L. Zhang, *Res. Chem. Intermed.*, 2014, **40**, 903–911.
16 A. Kaur and S. K. Kansal, *Chem. Eng. J.*, 2016, **302**, 194–203.
17 M. S. Gui and W. D. Zhang, *Nanotechnology*, 2011, **22**, 9.
18 T. Y. Han, X. Wang, Y. C. Ma, G. L. Shao, X. L. Dong and C. L. Yu, *J. Sol-Gel Sci. Technol*, 2017, **82**, 101–108.
19 P. Zhang, X. Teng, X. Feng, S. Ding and G. Zhang, *Ceram. Int.*, 2016, **42**, 16749–16757.
20 S. O. Alfaro and A. Martínez-de La Cruz, *Appl. Catal., A*, 2010, **383**, 128–133.
21 Y. Zhou, Z. P. Tian, Z. Y. Zhao, Q. Liu, J. H. Kou, X. Y. Chen, J. Gao, S. C. Yan and Z. G. Zou, *ACS Appl. Mater. Interfaces*, 2011, **3**, 3594–3601.
22 X. Wang, L. Chang, J. Wang, N. Song, H. Liu and X. Wan, *Appl. Surf. Sci.*, 2013, **270**, 685–689.
23 C. Zhang and Y. Zhu, *Chem. Mater.*, 2005, **17**, 3537–3545.
24 H. Huang, H. Chen, Y. Xia, X. Tao, Y. Gan, X. Weng and W. Zhang, *J. Colloid Interface Sci.*, 2012, **370**, 132–138.
25 T. Hu, H. Li, R. Zhang, N. Du and W. Hou, *RSC Adv.*, 2016, **6**, 31744–31750.
26 H. Zhou, Z. Wen, J. Liu, J. Ke, X. Duan and S. Wang, *Appl. Catal., B*, 2019, **242**, 76–84.
27 M. S. Gui, W. D. Zhang, Y. Q. Chang and Y. X. Yu, *Chem. Eng. J.*, 2012, **197**, 283–288.
28 S. Yao, J. Wei, B. Huang, S. Feng, X. Zhang, X. Qin, P. Wang, Z. Wang, Q. Zhang and X. Jing, *J. Solid State Chem.*, 2009, **182**, 236–239.
29 R. Senthil Kumar and P. Rajkumar, *Infrared Phys. Technol.*, 2014, **67**, 30–41.
30 A. Kljun, T. A. S. Benians, F. Goubet, F. Meulewaeter, J. P. Knox and R. S. Blackburn, *Biomacromolecules*, 2011, **12**, 4121–4126.
31 D. M. Chen, Q. Hao, Z. H. Wang, H. Ding and Y. F. Zhu, *Crystengcomm*, 2016, **18**, 1976–1986.
32 S. F. Chen, W. M. Tang, Y. F. Hu and X. L. Fu, *Crystengcomm*, 2013, **15**, 7943–7950.
33 Z. Q. Jia and C. N. Tian, *Desalination*, 2009, **247**, 423–429.
34 P. Goodman, R. Marks, C. Nexhip, T. A. O'Donnell and P. Miller, *Physica C*, 1993, **217**, 325–334.
35 H. Wang, Y. Liang, L. Liu, J. Hu and W. Cui, *Appl. Surf. Sci.*, 2017, **392**, 51–60.
36 X. Zhao, T. G. Xu, W. Q. Yao, C. Zhang and Y. F. Zhu, *Appl. Catal., B*, 2007, **72**, 92–97.
37 J. Shi, Y. Liang, Z. Li and B. Fang, *ChemistrySelect*, 2019, **4**, 5010–5018.
38 M. Malligavathy and P. D. Pathinettam, *Adv. Mater. Processes*, 2017, **2**, 51–55.
39 A. Rauf, M. S. A. Sher Shah, G. H. Choi, U. B. Humayoun, D. H. Yoon, J. W. Bae, J. Park, W. J. Kim and P. J. Yoo, *Adv. Mater. Processes*, 2015, **3**, 2847–2855.
40 T. Saison, P. Gras, N. Chemin, C. Chanéac, O. Durupthy, V. Brezova, C. Colbeau-Justin and J.-P. Jolivet, *J. Phys. Chem. C*, 2013, **117**, 22656–22666.
41 Y. Zhuo, J. Huang, L. Cao, H. Ouyang and J. Wu, *Mater. Lett.*, 2013, **90**, 107–110.
42 C. Wang, L. Zhu, C. Song, G. Shan and P. Chen, *Appl. Catal., B*, 2011, **105**, 229–236.
43 P. Xiao, L. Zhu, Y. Zhu and Y. Qian, *J. Solid State Chem.*, 2011, **184**, 1459–1464.
44 M. T. L. Lai, C. W. Lai, K. M. Lee, S. W. Chook, T. C. K. Yang, S. H. Chong and J. C. Juan, *J. Alloys Compd.*, 2019, **801**, 502–510.
45 S. Zhong, C. Li, M. Shen, C. Lv and S. Zhang, *J. Mater. Res. Technol.*, 2019, **8**, 1849–1858.
46 Z. Du, R. Guo, J. Lan, S. Jiang, C. Cheng, L. Zhao and L. Peng, *Fibers Polym.*, 2017, **18**, 2212–2218.
47 B. Liu, J. Wang, J. Wu, H. Li, Z. Li, M. Zhou and T. Zuo, *J. Mater. Chem. A*, 2014, **2**, 1947–1954.
48 L. Wang, G. Yang, D. Wang, C. Lu, W. Guan, Y. Li, J. Deng and J. Crittenden, *Appl. Surf. Sci.*, 2019, **495**, 143521.
49 L. Hao, L. Kang, H. W. Huang, L. Q. Ye, K. L. Han, S. Q. Yang, H. J. Yu, M. Batmunkh, Y. H. Zhang and T. Y. Ma, *Adv. Mater.*, 2019, **31**, 7.
50 L. Chang, F. Cao, J. Cai, W. Liu, J. Zhang and C. Cao, *Electrochem. Commun.*, 2009, **11**, 2245–2248.
51 A. Mihaylova, K. Hadjiivanov, S. Dzwigaj and M. Che, *J. Phys. Chem. B*, 2006, **110**, 19530–19536.
52 R. Kefirov, E. Ivanova, K. Hadjiivanov, S. Dzwigaj and M. Che, *Catal. Lett.*, 2008, **125**, 209.
53 Y. Tian, G. Hua, W. Xu, N. Li, M. Fang and L. Zhang, *J. Alloys Compd.*, 2011, **509**, 724–730.
54 M. Ge, Y. Li, L. Liu, Z. Zhou and W. Chen, *J. Phys. Chem. C*, 2011, **115**, 5220–5225.
55 M. Faisal, A. A. Ibrahim, H. Bouzid, S. Al Sayari, M. Al Assiri and A. A. Ismail, *J. Mol. Catal. A: Chem.*, 2014, **387**, 69–75.
56 T. Wang, F. Zhang, G. Xiao, S. Zhong and C. Lu, *Photochem. Photobiol.*, 2015, **91**, 291–297.
57 A. Phuruangrat, P. Dumrongrojthanath, N. Ekthammathat, S. Thongtem and T. Thongtem, *J. Nanomater.*, 2014, **2014**, 59.